Patchy percolation on a hierarchical network with small-world bonds

Stefan Boettcher* and Jessica L. Cook
Department of Physics, Emory University, Atlanta, Georgia 30322, USA

Robert M. Ziff†
Center for the Study of Complex Systems and Department of Chemical Engineering, University of Michigan, Ann Arbor, Michigan 48109-2136, USA

(Received 18 July 2009; published 13 October 2009)

The bond-percolation properties of the recently introduced Hanoi networks are analyzed with the renormalization group. Unlike scale-free networks, these networks are meant to provide an analytically tractable interpolation between finite-dimensional, lattice-based models and their mean-field limits. In percolation, the hierarchical small-world bonds in the Hanoi networks impose order by uniting otherwise disconnected, local clusters. This "patchy" order results in merely a finite probability to obtain a spanning cluster for certain ranges of the bond probability, unlike the usual 0–1 transition found on ordinary lattices. The various networks studied here exhibit a range of phase behaviors, depending on the prevalence of those long-range bonds. Fixed points in general exhibit nonuniversal behavior.

DOI: 10.1103/PhysRevE.80.041115 PACS number(s): 64.60.ah, 64.60.ae, 64.60.aq

I. INTRODUCTION

Percolation—the formation of a large connected component—is a geometric property in the arrangement of a many-body system that can strongly impact its physical behavior [1,2]. Typically, to observe any form of emergent, collective phenomena, an extensive fraction of the degrees of freedom must be sufficiently interconnected. Examples abound, from transport in amorphous materials [3] or the onset of plasticity in complex fluids [4] to the spreading of rumors or disease in social networks [5]. In particular, while percolation on regular and fractal lattice geometries [1] and ordinary random graphs [6,7] is a well-developed industry, its properties and impact of transport on the many conceivable forms of engineered networks (random, scale-free, etc) are just beginning to be explored [5,8,9].

Here, we study the percolation properties of the recently introduced set of Hanoi networks [10–12]. These networks mimic the behavior of small-world systems without the usual disorder inherent in the construction of such networks. Instead, they attain these properties in a recursive, hierarchical manner that lends itself to exact renormalization [13]. These networks do not possess a scale-free degree distribution [14–16]; they are, like the original Watts-Strogatz "small worlds" [17,18], of regular degree or have an exponential degree distribution. Yet, in turn the Hanoi networks have a more "physically" desirable geometry. In particular, they have the potential to provide an analytically tractable interpolation between finite-dimensional, lattice-based models and their mean-field limits, although no such interpolation will be considered here [11]. In our hierarchical scheme, the bond density is easily generalized to incorporate an arbitrary distance (i.e., hierarchy-)dependence, for instance, with a parameter corresponding to dimension [19]. Scale-free networks geared toward social phenomena or other lattices often used to analyze physical systems, such as the hierarchical lattice derived from the Migdal-Kadanoff bond-moving scheme [20–22], do not have a physically relevant mean-field behavior.

Many phenomena of interest in statistical physics, such as critical behavior, are fundamentally related to their percolation properties. We find that the renormalization group (RG) applied to percolation on the Hanoi networks behaves similar to that of a hierarchical lattice with small-world bonds and a scale-free degree distribution [23,24]. This is surprising, as this behavior has usually been associated with scale-free or nonequilibrium graphs [25]. Due to the hierarchical nature of the small-world bonds, the RG possesses unrenormalized parameters, which change the character of the RG flow in unusual ways. (For an early example of this effect, see Ref. [26].) In the exactly obtained phase diagrams, stable and unstable fixed points are drawn out into lines that often merge in branch points, generally making the scaling near fixed-points parameter-dependent and, hence, nonuniversal. As the flow can get attracted onto a stable line, mixed ordered-disordered phases appear in what we call "patchy" order: Otherwise isolated patches of localized clusters at low levels of the hierarchy get reconnected globally at higher levels with finite probability (depending on said parameters) to sustain long-range order. In the percolation problems discussed here, this manifests itself in the fact that the infinite network may percolate with a finite probability between zero and unity. (In conventional percolation, that probability has an instant 0–1 transition at the critical bond density p_c, although the size of the spanning cluster varies continuously, see Fig. 17 in Ref. [1].) A similar intermediate phase has been observed recently on an enhanced binary tree of bounded degree [27].

Our paper is structured as follows: In the next section, we review the construction of the Hanoi networks, followed by a pedagogical discussion of the renormalization group applied to percolation on hierarchical lattices with small-world bonds in Sec. III. Then, in Sec. IV we study the percolation prop-

*http://www.physics.emory.edu/faculty/boettcher/
†rziff@umich.edu

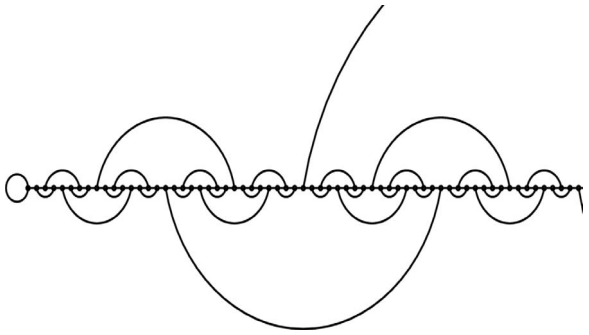

FIG. 1. Depiction of the three-regular network HN3 on a semi-infinite line. The entire graph becomes three-regular with a self-loop at $n=0$. Note that HN3 is planar.

erties of the Hanoi networks in some depth, and we conclude in Sec. V.

II. GEOMETRY OF THE HANOI NETWORKS

Each of the Hanoi network possesses a simple geometric backbone, a one-dimensional line of sites n, either infinite ($-2^k \le n \le 2^k$, $k \to \infty$), semi-infinite ($0 \le n \le 2^k$, $k \to \infty$), or closed into a ring of $N=2^k$ sites. Most importantly, all sites are connected to their nearest neighbors, ensuring the existence of the $1d$-backbone. To generate the small-world hierarchy in these networks, consider parameterizing any integer n (except for zero) *uniquely* in terms of two integers (i,j), via

$$n = 2^i(2j+1). \tag{1}$$

Here, $i \ge 0$ denotes the level in the hierarchy whereas j labels consecutive sites within each hierarchy. For instance, $i=0$ refers to all odd integers, $i=1$ to all integers once divisible by 2 (i.e., $2,6,10,\ldots$), and so on. In these networks, aside from the backbone, each site is also connected with (one or both) of its nearest neighbors *within* the hierarchy. For example, we obtain a 3-regular network HN3 (best done on a semi-infinite line) by connecting first the backbone, then 1–3, 5–7, 9–11, etc., for $i=0$, next 2–6, 10–14, etc., for $i=1$, and 4–12, 20–28, etc., for $i=2$, and so on, as depicted in Fig. 1. (The corresponding four-regular network HN4 [10], which we will not study here, is obtained in the same manner but connecting to *both* nearest neighbors in the hierarchy, i.e., 1–3, 3–5, 5–7, etc., for $i=0$, 2–6, 6–10, etc., for $i=1$, and so forth.)

Previously [10], it was found that the average chemical path between sites on HN3 scales with the distance l as

$$d^{HN3} \sim \sqrt{l} \tag{2}$$

along the backbone. In some ways, this property is reminiscent of a square lattice consisting of N lattice sites, whose diameter (=diagonal) is also $\sim\sqrt{N}$.

While HN3 (and HN4 [10]) are of a fixed, finite degree, we introduce here convenient generalizations of HN3 that lead to revealing insights into small-world phenomena. First, we can extend HN3 in the following manner to obtain a planar network of average degree 5, hence called HN5, at the price of a distribution in the degrees that is exponentially

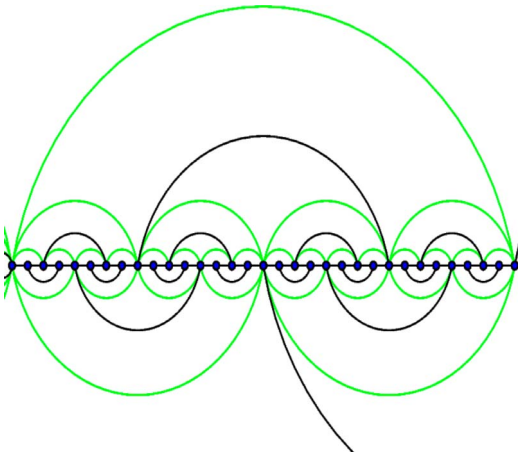

FIG. 2. (Color online) Depiction of the planar network HN5, comprised of HN3 (black lines) with the addition of further long-range bonds (green/shaded lines). There is no distinction made between black and shaded lines in our studies here.

falling. In addition to the bonds in HN3, in HN5 we also connect all even sites to both of their nearest neighboring sites that are *within* the same level of the hierarchy $i \ge 1$ in Eq. (1). The resulting network remains planar but now sites have a hierarchy-dependent degree, as shown in Fig. 2. To obtain the average degree, we observe that $\frac{1}{2}$ of all sites have degree 3, $\frac{1}{4}$ have degree 5, $\frac{1}{8}$ have degree 7, and so on, leading to an exponentially falling degree distribution of $\mathcal{P}\{\alpha=2i+3\} \propto 2^{-i}$. Then, the total number of bonds L in the system of size $N=2^k$ is

$$2L = 2k - 1 + \sum_{i=0}^{k-1} (2i+3)2^{k-1-i} = 52^k - 6. \tag{3}$$

And, thus, the average degree is

$$\langle \alpha \rangle = \frac{2L}{N} \sim 5. \tag{4}$$

In HN5, the end-to-end distance is trivially 1 (see Fig. 2). Therefore, we define as the diameter the largest of the shortest paths possible between any two sites, which are typically odd-index sites furthest away from long-distance bonds. For the $N=32$ site network depicted in Fig. 2, for instance, that diameter is 5, measured between site 3 and 19 (starting with $n=0$ as the leftmost site), although there are many other such pairs. It is easy to show recursively that this diameter grows strictly as

$$d^{HN5} = 2\lfloor k/2 \rfloor + 1 \sim \log_2 N. \tag{5}$$

We have checked numerically that the *average* shortest path between any two sites appears to increase logarithmically with system size N as well.

The networks HN3 and HN5 have the convenient but (from a mean-field perspective) unrealistic restriction of being planar. In fact, with a minor extension of the definition, it is easy to also design Hanoi networks that are both nonplanar *and* fully renormalizable. The simplest such network, which

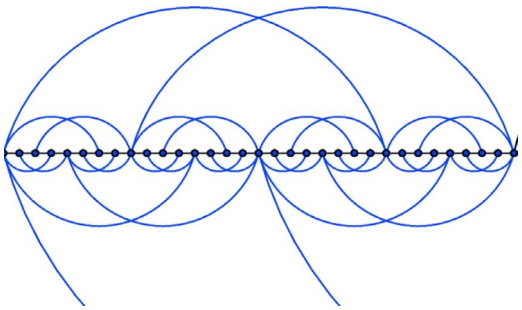

FIG. 3. (Color online) Depiction of the nonplanar Hanoi network HN-NP. Again, starting from a $1d$-backbone (black lines), a set of long-range bonds (blue/shaded lines) is added that break planarity but maintain the hierarchical pattern set out in Eq. (1). The RG on this network remains exact.

we dub HN-NP here, is depicted in Fig. 3. (Extensions will be introduced in Ref. [28].)

To obtain the average degree, we observe that $\frac{1}{2}+\frac{1}{4}$ of all sites have degree 3, $\frac{1}{8}$ has degree 5, $\frac{1}{16}$ has degree 7, and so on, leading to an exponentially falling degree distribution, as for HN5. The total number of bonds L in the system of size $N=2^k$ is

$$2L = 32^{k-1} + \sum_{i=2}^{k-1} (2i-1)2^{k-i} + 2k + (2k-2) = 42^k - 4. \tag{6}$$

And, thus, the average degree is

$$\langle \alpha \rangle = \frac{2L}{N} \sim 4. \tag{7}$$

Here, too, it is easy to see that the shortest paths between sites increases logarithmically with system size N.

III. RG FOR PERCOLATION

The principles of the renormalization group (RG) for percolation as it will be use in this paper are easiest to explain for a simple hierarchical lattice [22,23]. (Percolation on these hierarchical lattices has recently also been discussed in Ref. [24].) In this recursively constructed lattice, bonds from a preceding generation g are built up in the next generation $g+1$ according to a fixed pattern, until the complete network is constructed at a generation $g=k\to\infty$. Applying real-space renormalization to the complete network in effect reverses the recursive built-up of the network. The complete network with the "bare" operators obtained in the $g=k$th generation provides the initial conditions, or the $n=0$th step in the RG, which we evolve to $n\to\infty$ (i. e., $k\to\infty$) and study the fixed points of this recursion and their stability.

An example of this is shown in Fig. 4 for the first three generations $(g=0,1,2)$ of a hierarchical lattice that corresponds to a one-dimensional line (solid bonds) with a hierarchy of small-world bonds (dashed lines) [23]. It is fruitful to regard both types of bonds as distinct at this stage, although in any complete network one may be interested

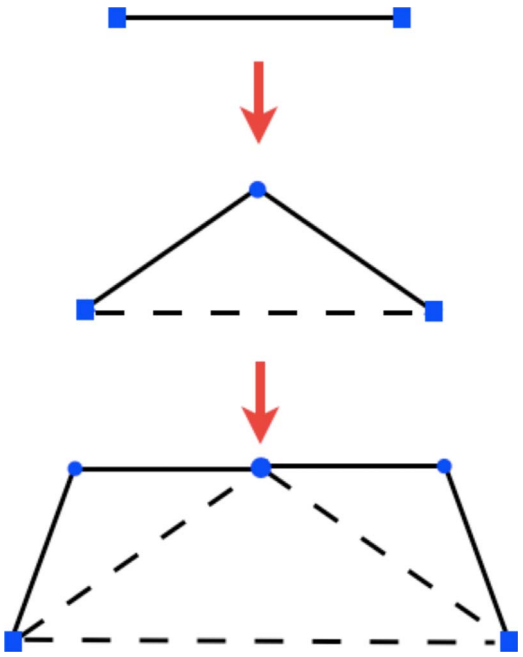

FIG. 4. (Color online) Pattern for the recursive generation of a hierarchical lattice. In zeroth generation (top), the lattice consists of a single bond between the two "boundary" sites (squares). In successive generations each bond of that type (solid line) is replaced by a new type of bond (dashed line) in parallel with a sequence of two of the original bonds (solid lines), see middle and bottom for generation one and two.

mostly in the case where all bonds are indistinguishable and exist with equal probability in the context of percolation, say.

In Fig. 5, we list all eight graphlets consisting of those three bonds. Summing the weights of those five graphlets that connect end-to-end and, thus, contribute to the percolation probability q_{n+1}, we obtain

$$q_{n+1} = p + (1-p)q_n^2. \tag{8}$$

It should be noted that there is no corresponding recursion for the small-world bond p (dashed line). It enters the RG anew at each step, bare and unrenormalized. (As we will see, this feature is a defining characteristic also of RG in the Hanoi networks, as discussed in Ref. [10].)

It is very simple, or course, to obtain the fixed points of the RG in Eq. (8) in the thermodynamic limit $k\to\infty$ with the Ansatz $q_{n+1}=q_n=q^*$ for $n\to\infty$. Our case yields the trivial unstable fixed point $q^*=1$ and a nontrivial but *stable* fixed point at

$$q^*(p) = \frac{p}{1-p} \quad \left(p \le \frac{1}{2}\right). \tag{9}$$

We have obtained a line of stable fixed points depending on the parameter p. For $p=0$, we obtain the ordinary and trivial percolation problem of a one-dimensional lattice with a percolation threshold at $q_c=1$: For any initial bond probability $q_0<1$, the RG flow from the recursion in Eq. (8) evolves away from the unstable fixed point $q^*=1$ to the stable fixed point $q^*=0$. The ordered (percolating) state is attained only

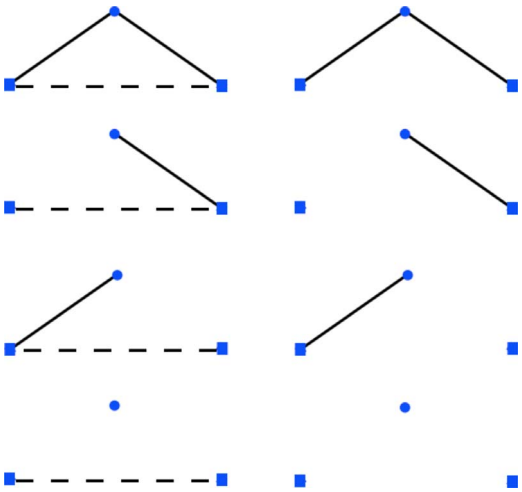

FIG. 5. (Color online) All possible combinations of reducing bonds from the n-th RG step to form a new bond at step $n+1$, reversing the pattern set in Fig. 4. All graphs on the left percolate (i.e., connect end-to-end) by merit of the dashed bond alone, while on the right only the top graph provides such a connection. If q_n is the probability for a solid and p for a dashed bond, the weights for the graphs on the left are pq_n^2, $pq_n(1-q_n)$, $pq_n(1-q_n)$, and $p(1-q_n)^2$ and on the right are $(1-p)q_n^2$, $(1-p)q_n(1-q_n)$, $(1-p)q_n(1-q_n)$, and $(1-p)(1-q_n)^2$ from top to bottom.

for $q_0=1$. For all $p \geq 0$, the phase diagram for the RG flow is shown in Fig. 6. For any $p<\frac{1}{2}$, the usual ordered state remains confined to the unstable fixed point $q_0=q^*=1$. For any other starting value $0 \leq q_0<1$, the RG flow converges onto the line of nontrivial stable fixed points given by Eq. (9) in which the usual nonpercolating, disordered state is now replace by a *partially ordered* state, i. e., even in the thermodynamic limit there is a *finite* probability to percolate. For $p \geq \frac{1}{2}$, the stable and unstable fixed points merge and an ordered, percolating state is reached irrespective of q_0 (even when it vanishes), merely by the strength of the small-world bond, which repeatedly, at any generation of the hierarchical lattice, has a chance p to rectify any nonpercolating sublattices from previous generations (see, for instance, the bottom network in Fig. 4). In reference to the corresponding effect we found previously for the Ising ferromagnet on HN5, we call this partially ordered state "patchy" [28]: ordering occurs between the lucky neighborhoods that happen to be connected by the occasional small-world bond.

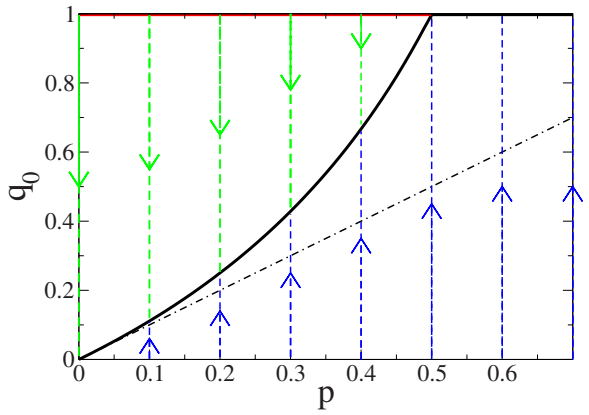

FIG. 6. (Color online) Phase diagram for the RG flow of the simple hierarchical lattice due to Eq. (8). For any given p, the flow for q_n evolves along the flow trajectories starting from a chosen initial value q_0. Except for points ($p<\frac{1}{2}$, $q_0=1$) on the (thick red/shaded) line of unstable fixed points, all points ($p, q_0<1$) flow toward the (thick black) line of stable fixed points from Eq. (9) or $q^*=1$ for $p>\frac{1}{2}$. This is especially true for a homogeneous choice of bond probabilities in a network, $q_0=p$ along the (dash-dotted) diagonal line.

We obtain this picture from a local analysis of Eq. (8) near the fixed point with the Ansatz

$$q_n \sim q^* - \delta_n \tag{10}$$

assuming $\delta_n \ll 1$. To leading order with $q^*=1$ yields

$$\delta_{n+1} \sim 2(1-p)\delta_n \tag{11}$$

with solution

$$\delta_n \sim [2(1-p)]^n \delta_0. \tag{12}$$

For $2(1-p)<1$, the corrections δ_n contract for increasing n, leaving the fixed point stable. In contrast, for $2(1-p)>1$ the corrections escalate (eventually violating the assumption) and the fixed point is said to be unstable. As shown in Fig. 6, the line of unstable fixed points at $q^*=1$ for small p thus disappears at $\bar{p}=\frac{1}{2}$ and is replaced by a stable fixed point at all larger p.

Typically, in a complete network, we make no distinction between the probabilities of any of the bonds in the network, whether they are small-world or not. Hence, in light of Fig. 6, the RG flow would initiate with $q_0=p$, which corresponds to the flow trajectories emanating from the diagonal (dash-dotted) line. Consequently, projecting the flow in the diagram just onto that diagonal, one would conclude that there is no conventional phase transition. Starting on the open diagonal at any point the flow proceeds to a larger effective percolation probability. There is an interesting transition in this behavior at $\bar{p}=\frac{1}{2}$ between a fully ordered (percolating) phase above, where this flow always converges to $q^*=1$, and a partially ordered, patchy phase below, converging to some nontrivial value of $q^*=q^*(p=q_0)<1$ given by Eq. (9). We will see that this situation resembles very closely that of percolation on HN5. Notice that the unstable fixed point discussed above, typically itself the focus of any study in critical phenomena, seems to have become irrelevant to these considerations, as our initial conditions never cross an unstable manifold.

It is, in fact, just as simple to analyze the corresponding behavior for the small-world hierarchical network on an underlying two-dimensional lattice [23]. As shown in Fig. 7, we merely need to add a second sequence of two (solid line) bonds to the previous hierarchical generation of the network in Fig. 4, resulting in a new graphlet of five bonds. As in Fig. 5, we consider the now $2^5=32$ graphlets regarding the end-to-end connectivity and sum the weights of those that contribute to percolation. Analogous to one-dimensional RG recursion (8) we find

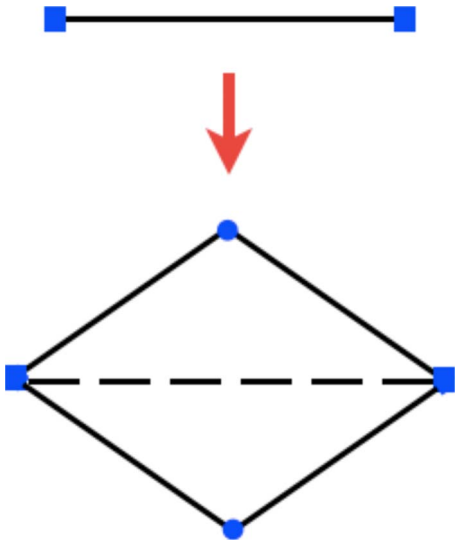

FIG. 7. (Color online) Pattern for the recursive generation of a $2d$ hierarchical lattice, originating from the Migdal-Kadanoff bond-moving scheme in a square lattice, with the addition of a small-world bond. Each single, solid bond between the two sites (squares) of a previous generation is replaced by a small-world bond (dashed line) in parallel with two sequences of two of the original bonds (solid lines) at the next generation.

$$q_{n+1} = p + (1-p)q_n^2(2-q_n^2), \tag{13}$$

which is very similar in character: it also depends on a non-renormalized, bare parameter p for the probabilities of the small-world bond at every recursion. The same fixed-point analysis as above leads to a more complex but straightforward algebraic equation for $q^*=q^*(p)$, and we plot the respective RG flow in Fig. 8. Without small-world bonds, at $p=0$, we already observe the emergence of a nontrivial unstable fixed of the ordinary two-dimensional hierarchical lattice at $q^*=1/\phi=0.618\ldots$, where $\phi=(\sqrt{5}+1)/2$ is the "golden ratio" [29]. In this case, $q^*(p)$ develops a remarkable branch-point singularity within the physical domain at the critical point $\bar{p}=\frac{5}{32}$, where two branches of fixed points pinch off into the complex plane and the stable fixed point attained for all points along the diagonal $q_0=p$ jumps discontinuously from $q^*(p\to\bar{p}^-)=\frac{1}{3}$ to $q^*(p\to\bar{p}^+)=1$.

Again, we can verify these findings with a local analysis along the line of fixed points with the same Ansatz as in Eq. (10), where $q^*(p)$ is now a solution of Eq. (13) (see the parabolic line in Fig. 8). We obtain

$$\delta_{n+1} \sim 4(1-p)q^*[1-(q^*)^2]\delta_n, \tag{14}$$

where the simultaneous solution of the fixed-point equation together with the stability condition on the Ansatz,

$$4(1-p)q^*[1-(q^*)^2] < 1, \tag{15}$$

defines the branch of stable fixed points, while its violation implies the unstable branch. Both branches meet when the inequality in Eq. (15) is saturated, at $\bar{p}=\frac{5}{32}$ and $q^*=\frac{1}{3}$. The fixed-point analysis for $q^*=1$ leads to

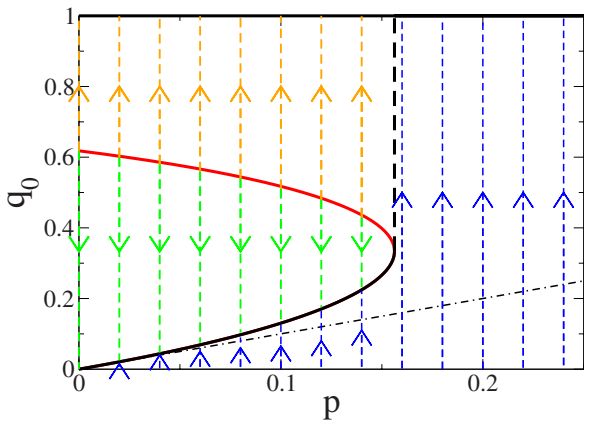

FIG. 8. (Color online) Phase diagram for the RG flow of the $2d$ hierarchical lattice due to Eq. (13), using the same notation as in Fig. 6. Here, there exists an additional phase for $p<\bar{p}=\frac{5}{32}=0.15625$ due to the (thick red/shaded) line of unstable fixed points on some line $q_0(p)<1$. Points above that line flow into the now stable ordered fixed point $q^*=1$. Note that for the homogeneous choice of bond probabilities in a network, i.e., $q_0=p$ along the (dash-dotted) diagonal line, we observe a discontinuous behavior at $\bar{p}$: Rising from the partially ordered phase below, the flow onto a finite percolation probability $q^*<1$ jumps (along the thick dashed vertical line) to $q^*=1$ in the fully ordered phase above $\bar{p}$.

$$\delta_{n+1} \sim 4(1-p)\delta_n^2. \tag{16}$$

This nonlinear relation has the solution

$$\delta_n \sim \frac{1}{4(1-p)}[4(1-p)\delta_0]^{2^n}. \tag{17}$$

Deriving from our assumption, it is certainly true that $\delta_0<\frac{1}{4}$ and hence δ_n vanishes and the fixed point proves to be exceedingly attractive and stable, ever more so for increasing p.

IV. RG FOR PERCOLATION ON HANOI NETWORKS

In this section, we study percolation on HN3, HN5, and HN-NP with the renormalization group. It is easy to convince oneself that percolation on HN3 can only occur at full connectivity $p\to 1$ because HN3 is finitely ramified: To prevent end-to-end connectivity or the emergence of a giant component only a fixed number of bonds need to be cut at *any* system size [1]. This is most apparent by plotting HN3 as a branched Koch curve (see Fig. 9). Yet, the limit $p\to 1$ in HN3 itself is interesting, showing logarithmic finite-size corrections, which appear impossible to resolve numerically. Moreover, the derivation of the RG recursions for HN3 are almost identical to that for HN5 and HN-NP, which in turn have a more interesting phase diagram.

A. Renormalization Group Studies for HN3

First, we consider the renormalization group for end-to-end percolation on HN3. In this case, all steps can be done exactly. Following Taitelbaum *et al.* [30] in their analysis of the Sierpinski gasket, the RG step consists of eliminating

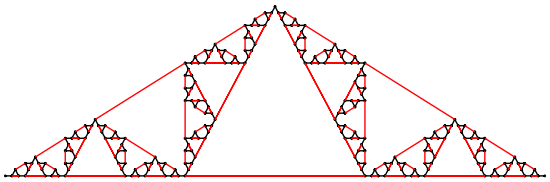

FIG. 9. (Color online) Representation of HN3 as a branched Koch curve. The one-dimensional backbone shown in Fig. 1 is marked in black here; long-range bonds are in red/shaded. In this representation, the diameter in Eq. (2) corresponds to the baseline in the Koch curve. To prevent end-to-end connectivity, only two bonds right down the symmetry axis need to be cut, independent of size. Hence, the network is finitely ramified.

every second (odd) site in the network and calculating new, renormalized probabilities for connections between the remaining sites, as explained in Fig. 10. Four independent probabilities (R_n, S_n, T_n, U_n) are evolved under RG; the fifth probability, N_n, follows from conservation of probability.

We obtain a system of RG recursion equations, in which the renormalized probabilities $(R_{n+1}, S_{n+1}, T_{n+1}, U_{n+1})$ are functions of $(R_n, S_n, T_n, U_n; p)$. As for the case of the hierarchical lattices in Sec. III, these equations are unusual, as they retain a *memory* of the original bond probability p for all times, which enters as a source term through the dependence on the next level in the hierarchy [10]. The initial conditions can be read off the right graphlet in Fig. 10. Unlike in the other sections, where we merely execute a local stability analysis near fixed points, here we need to make contact with the initial conditions in the analysis to explore finite-size corrections. Therefore, we follow again the notation in Ref. [30] and shift the RG recursion to evolve from initially $n=-k$ to terminate at $n=0$ for a system of size $L=2^k$ in the thermodynamic limit $k\to\infty$. Originally there is no bond ac, thus $U_{-k}=0$ and $R_{-k}=p^2$ because it only consists of having both, ab and bc, connected. We have $S_{-k}=T_{-k}=p(1-p)$ for an exclusive ab or bc connection, respectively; hence $N_{-k}=(1-p)^2$.

We determine the form of the recursion equations for these probabilities by a simple counting procedure, as explained in Fig. 11. We find

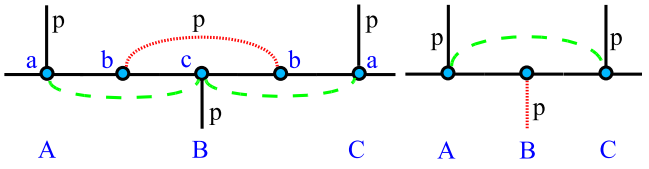

FIG. 10. (Color online) Depiction of the (exact) renormalization-group step for percolation on HN3. The step consists of eliminating every second site (with label b) in the left diagram and expressing the renormalized connection probabilities $(R_{n+1}, S_{n+1}, T_{n+1}, U_{n+1}, N_{n+1})$ on the right diagram in terms of the old values $(R_n, S_n, T_n, U_n, N_n)$. Here, R_n refers to the probability that three consecutive points abc are connected, S_n refers to ab being connected but not c, T_n to bc being connected but not a, U_n to ac being connected but not b, whereas N_n refers to the probability that neither a, b, or c are mutually connected. Upper case letters A, B, C refer to the renormalized sites at $n+1$. Note that the original network in Fig. 1 does not contain bonds of type U_n (long-dashed line), but that they become relevant during the RG process.

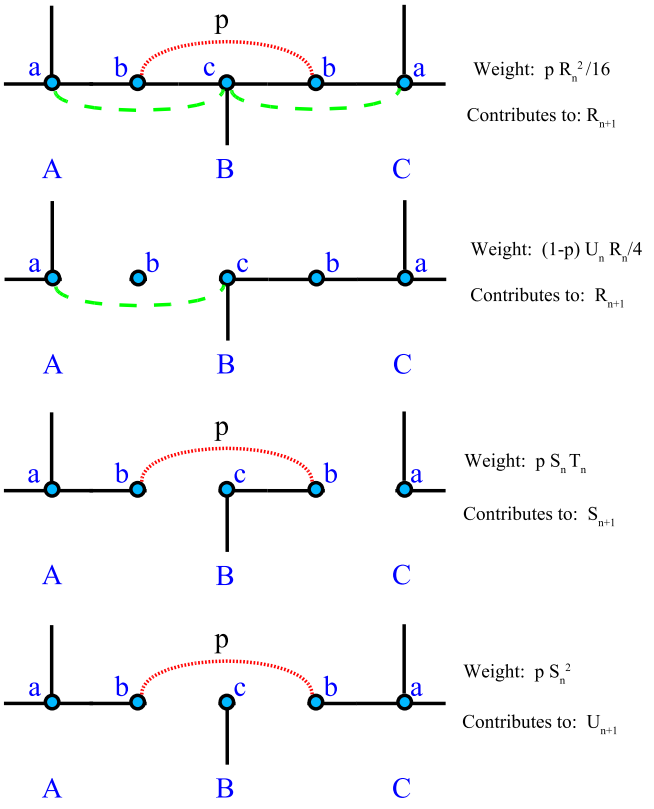

FIG. 11. (Color online) Example of graphlets contributing to the RG step in HN3. Eliminating every second site in the network (dots labeled b), the connectedness of the renormalized sites (A, B, C) have to be assessed. There are seven bonds in the elementary graphlet: two each for pair connections ab, bc, and ac, and one previously unrenormalized bond with raw probability p stretching between the two sites b. Bonds of higher level in the hierarchy (vertical lines) remain *unaffected* until a later RG step. Thus, $2^7=128$ graphlets with combinations of these bond must be considered. Only four examples are displayed here. In the first, all bonds are present with a direct bond between abc on both sides of B; each such triangle has a probability $R_n/4$, and the bond p is present, making the weight $pR_n^2/16$. Because, after renormalization, the remaining sites ABC are also directly linked, this graphlet contributes to R_{n+1}. In the second example, only ac but not b are linked on the left, contributing a weight of U_n, but there is a path connecting abc on the right with weight $R_n/4$, and there is no bond p, making the total weight $(1-p)U_nR_n$. Again, there is a path between ABC, so it contributes to R_{n+1}. In the third example, the S_n bond between ab on the left and the T_n bond on the right together with the p-bond ensure a connection between AB, thus making a contribution to S_{n+1}. The fourth example is the only graphlet that contributes to U_{n+1} with a direct link between AC but not B.

$$R_{n+1} = R_n^2 + 2U_nR_n + U_n^2 + 2pS_nR_n,$$

$$S_{n+1} = R_nT_n + R_nN_n + U_nN_n + U_nT_n + U_nS_n + pS_nT_n + (1-p)R_nS_n,$$

$$T_{n+1} = R_nT_n + R_nN_n + U_nN_n + U_nT_n + U_nS_n + pS_nT_n + (1-p)R_nS_n,$$

$$U_{n+1} = pS_n^2,$$

$$N_{n+1} = T_n^2 + 2N_nS_n + 2N_nT_n + N_n^2 + 2(1-p)S_nT_n + (1-p)S_n^2. \tag{18}$$

Note that unlike for the Sierpinski gasket [30] but similar to Eqs. (8) and (13), the RG depends explicitly on p at every recursion, not merely through the initial conditions.

Obviously, the equations imply that $T_n = S_n$ for all n, making the T operator redundant. Combining probabilities S_n and T_n into a single probability S_n for having a connection between either ab or bc, and rescaling by a factor of $\frac{1}{2}$, Eq. (18) can be simplified to

$$R_{n+1} = (R_n + U_n)^2 + pS_nR_n,$$

$$S_{n+1} = 2(S_n + U_n)(R_n + U_n) + \frac{p}{2}S_n^2 - pR_nS_n,$$

$$U_{n+1} = \frac{1}{4}pS_n^2,$$

$$N_{n+1} = (S_n + N_n)^2 - \frac{3}{4}pS_n^2, \tag{19}$$

which satisfies the constraint

$$1 = N_n + R_n + S_n + U_n \tag{20}$$

for all n. The initial conditions at $n=-k$ are now

$$R_{-k} = p^2,$$

$$S_{-k} = 2p(1-p),$$

$$U_{-k} = 0,$$

$$N_{-k} = (1-p)^2. \tag{21}$$

Note that the fixed-point equations can be solved exactly for arbitrary p, as they involve the solution of three coupled quadratic equations, but the expressions are extremely complex. Instead, we search for fixed points of these equations numerically. For any physical p inside the unit interval we find *no* physical fixed points with $0 < N^*$, R^*, S^*, $U^* < 1$.

The analysis of RG recursion Eq. (19) proceeds as follows. The obligatory trivial fixed points, i. e., stationary solutions of Eq. (19), at $(N^*, R^*, S^*, U^*) = (1,0,0,0)$ and (0,1,0,0) exist for any p. We search for a nontrivial fixed point by choosing a value of $0 < p < 1$, and numerically evolve Eq. (19) for that value of p, starting from the initial conditions in Eq. (21). We find that for all values of p, the equations evolve toward the stable fixed point at (1,0,0,0), characteristic for a completely disconnected network, although this evolution takes ever longer, the closer p is to unity. Therefore, we conclude

$$p_c = 1. \tag{22}$$

This result is not too surprising, because this network is of finite ramification: a bounded number of cuts can separate the network into two extensive pieces. Finitely ramified objects, such as the triangular Sierpinski gasket, can only percolate with certainty at full connectivity, $p_c = 1$. Corrections to this behavior in HN3 are more interesting and, in fact, decay *faster* for $k \to \infty$ than for other finitely ramified objects like the Sierpinski gasket.

First-order correction to $p_c = 1$

To determine the finite-size corrections for $p_c = 1$, we expand around the *unstable* fixed point (0,1,0,0) to first order with the Ansatz

$$R_n \sim 1 - r_n^{(1)}, \quad (r_n^{(1)} \ll 1),$$

$$S_n \sim s_n^{(1)}, \quad (s_n^{(1)} \ll 1),$$

$$U_n \sim u_n^{(1)}, \quad (u_n^{(1)} \ll 1),$$

$$N_n \sim \eta_n^{(1)}, \quad (\eta_n^{(1)} \ll 1). \tag{23}$$

Inserting into Eq. (19) and dropping terms beyond first order, we obtain immediately that

$$u_n^{(1)} = \eta_n^{(1)} = 0. \tag{24}$$

The norm in Eq. (20) implies $1 \sim 1 - r_n^{(1)} + s_n^{(1)}$, i.e.,

$$r_n^{(1)} = s_n^{(1)} \tag{25}$$

and we get from the equations in Eq. (19) for S_{n+1},

$$s_{n+1}^{(1)} \sim (2-p)s_n^{(1)}, \tag{26}$$

which together with Eq. (25) have the consistent solution

$$r_n^{(1)} = s_n^{(1)} \sim A(2-p)^n. \tag{27}$$

Applying the initial conditions in Eq. (21), we can now assess the finite-size corrections to $p_c = 1$ with the Ansatz

$$p \sim 1 - \epsilon_k, \quad (\epsilon_k \ll 1). \tag{28}$$

Inserting this and the result for $r_{-k}^{(1)}$ and $s_{-k}^{(1)}$ in Eq. (27) into Eq. (21) yields a consistent result, which is

$$A(1+\epsilon_k)^k \sim 2\epsilon_k. \tag{29}$$

Note also that with p in Eq. (28), the last initial condition in Eq. (21) evaluates consistently to $N_{-k} = O(\epsilon_k^2)$.

To leading order, we obtain from Eq. (29)

$$\epsilon_k \sim \frac{\ln k}{k}, \tag{30}$$

independent of the unknown constant A. In general it would be best to extract ϵ_k directly from Eq. (29) for any given k, as Eq. (30) is poorly convergent. Unfortunately, though, we have not found a way to fix A in this local expansion. We conclude here by noting that the leading corrections to $p_c = 1$ as stated in Eq. (30) decays faster than what Ref. [30] found for the Sierpinski gasket, $\epsilon_k \sim 1/(2\sqrt{k})$, where $k = \log_2 N$. We continue with the second-order correction in the Appendix, with the final result given in Eq. (57).

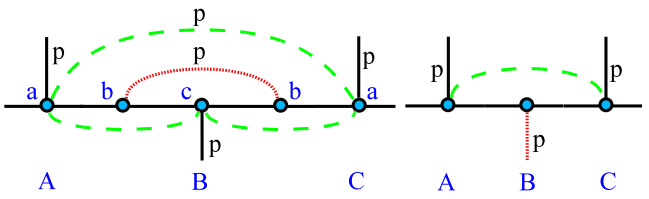

FIG. 12. (Color online) Depiction of the (exact) RG step for percolation on HN5. In contrast to the corresponding step for HN3 in Fig. 10, the long-dashed bonds are germane to the network, not emergent properties. Thus, the long-dashed bond on top (left) has still probability p; the long-dashed bonds of the previous hierarchical level below have a probability of p plus the emergent contribution from the previous step. The graphlet after the RG step (right) is identical to that in Fig. 10.

B. RG for HN5

Just as HN5 is a simple extension of HN3, see Sec. II above, so is the analysis of the percolation problem. Yet, the added bonds in HN5 precisely rectify the finite ramification that made the percolation phase diagram for HN3 trivial. On the face of it, it is not entirely obvious that percolation on HN5 would be any more interesting, because its ramification is only marginally infinite. Now the number of lines to be cut grows logarithmically with size $N=2^k$ because each new level k of the hierarchy adds another end-to-end connection (see Fig. 2).

The RG step for HN5 involves merely one extra bond in the elementary graphlet (see Fig. 12). The derivation of the RG recursion equations is similar to Eq. (19); however, we now have to evaluate twice as many graphlets. But one half of the graphlets—those without the new line—simply correspond exactly to those of HN3 in weight (times a factor of $1-p$) and in the operator to which they contribute. The other half again have the same weight (times a factor p, for the now-present new bond), but the additional bond changes the operator to which these graphlets contribute in 69 out of the 128 cases by adding extra connectivity. These considerations and the corresponding discussion along the lines of Sec. IV A lead to

$$R_{n+1} = (R_n + U_n)^2 + 2p(S_n + N_n)(R_n + U_n) + p(1-p)S_nR_n + \frac{p^2}{2}S_n^2,$$

$$S_{n+1} = 2(1-p)\left[(S_n + N_n)(R_n + U_n) + \frac{p}{4}S_n^2\right] - p(1-p)R_nS_n,$$

$$U_{n+1} = p\left[(S_n + N_n)^2 + \frac{1-3p}{4}S_n^2\right],$$

$$N_{n+1} = (1-p)\left[(S_n + N_n)^2 - \frac{3}{4}pS_n^2\right], \tag{31}$$

which again satisfies the norm constraint in Eq. (20). The initial conditions are now

$$R_0 = p^2(3-2p),$$

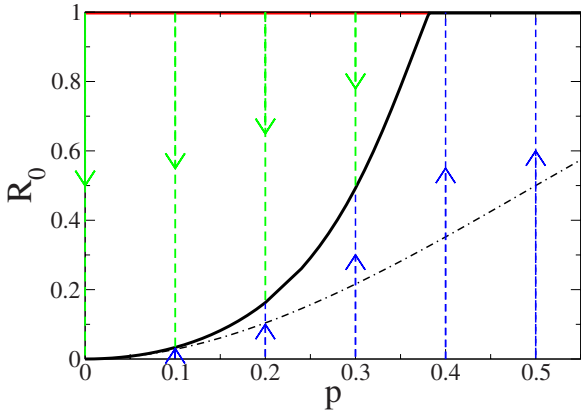

FIG. 13. (Color online) Phase diagram for the RG flow of HN5 due to Eq. (31). The all-connected operator R is used as an indicator of percolative order in the system. For any given p, R_n evolves along the shown trajectories starting from an initial value R_0. Except for points ($p<\bar{p}=2-\phi$, $R_0=1$) on the (thick red/shaded) line of unstable fixed points, all points ($p, R_0<1$) flow toward the (thick black) line of stable fixed points obtained from Eq. (31) or to $R^*=1$ for $p>\bar{p}$. For a homogeneous choice of bond probabilities in the network given in Eqs. (32), i.e., $R_0=p^2(3-2p)$ on the dash-dotted line, the stable fixed point is always approached from below.

$$S_0 = 2p(1-p)^2,$$

$$U_0 = p(1-p)^2,$$

$$N_0 = (1-p)^3. \tag{32}$$

The algebraic fixed-point equations obtained from Eq. (31) for $n \approx n+1 \to \infty$ are of a high polynomial order. It is easy to establish the fixed point at $(N^*, R^*, S^*, U^*) = (0,1,0,0)$ for any p. But the other trivial stable fixed point at $(N^*, R^*, S^*, U^*) = (1,0,0,0)$, describing the disordered state, *only* exists at $p=0$. Instead, we find (numerically, as the solution of a sixth-order polynomial) a nontrivial equation for a line of fixed point which merges into the fully ordered, percolating fixed point $R^*=1$ that is stable for all $p>\bar{p}=2-\phi=0.381966\ldots$, where $\phi=(\sqrt{5}+1)/2$. The resulting phase diagram in Fig. 13 is very similar to that in Fig. 6 for the hierarchical small-world lattice. The difference is that HN5 is more mean-field-like in the sense of ordinary random graphs, with an exponential instead of a scale-free degree distribution.

We obtain the value for $\bar{p}$ explicitly from the analysis of the fixed point at $R^*=1$. In fact, we proceed similar to Sec. IV A by applying the same Ansatz in Eq. (23) to the RG recursions in Eq. (31). A first-order expansion yields

$$r_n^{(1)} = s_n^{(1)},$$

$$s_{n+1}^{(1)} \sim (2-p)(1-p)s_n^{(1)}, \tag{33}$$

with $u_n^{(1)} = \eta_n^{(1)} \equiv 0$. Finally, we have

$$r_n^{(1)} = s_n^{(1)} \sim A[(2-p)(1-p)]^n. \tag{34}$$

Despite the obvious similarity to Eqs. (23)–(27), the key difference of the solution in Eq. (34) is that there is a nontrivial

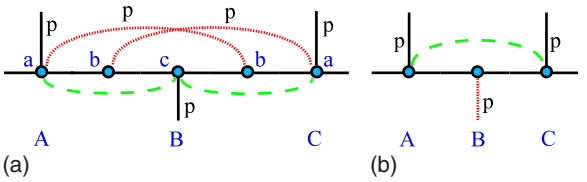

FIG. 14. (Color online) Depiction of the (exact) RG step for percolation on HN-NP. In contrast to HN3, the long-range bond connecting *bb* in Fig. 10 is replaced by a crossing pair of such bonds connecting *ab*. The *U* bond connecting *ac* is an emergent operator, like in HN3. The graphlet after the RG step (right) is identical to that for HN3 (5) in Fig. 10 (12).

transition at $\bar{p}=2-\phi$, derived from the marginal stability condition,

$$1 = (2-\bar{p})(1-\bar{p}) \tag{35}$$

such that the fixed point is unstable for $0 \le p < \bar{p}$ and stable for $\bar{p} < p \le 1$. Clearly, the approach to the fixed point is highly parameter dependent, leading to nonuniversality such as in the correlation-length exponent for $p < \bar{p}$ [13],

$$\nu = \frac{\ln 2}{\ln[(2-p)(1-p)]}. \tag{36}$$

C. Percolation in HN-NP

A more substantial extension to the previous planar Hanoi networks is given by HN-NP introduced in Sec. I (see Fig. 3). It extends the basic network-building concept into the nonplanar regime while preserving exact renormalizability. The single, long-range bond of HN3 in the elementary graphlet in Fig. 10 is here replaced by a pair of crossing small-world bonds, as explained in Fig. 14. As the second diagram shows, the graphlet resulting from the RG step is *identical* to those for HN3 and HN5. As in HN3, only the *U* operator that connect sites *ac* exclusively emerges anew during the RG recursion. (Elsewhere, we also consider that operator as pre-existing for HN-NP, the same step that converts HN3 into HN5 [28].)

Evaluation of the $2^8=256$ elementary graphlets as described in connection with Fig. 11 above results in the recursion equations

$$R_{n+1} = (R_n + U_n)^2 + p(3-p)R_nS_n + 2pR_nN_n + pS_nU_n + \frac{3}{4}p^2S_n^2,$$

$$S_{n+1} = (2-p)[(1-p)R_n + U_n]S_n + 2(1-p)R_nN_n + 2U_nN_n + pN_nS_n + p(1-p)S_n^2,$$

$$U_{n+1} = p\left(1-\frac{3}{4}p\right)S_n^2 + pN_nS_n,$$

$$N_{n+1} = N_n^2 + 2(1-p)S_nN_n + (1-p)^2S_n^2, \tag{37}$$

obeying the normalization constraint in Eq. (20), and with the same initial conditions as for HN3 in Eq. (21).

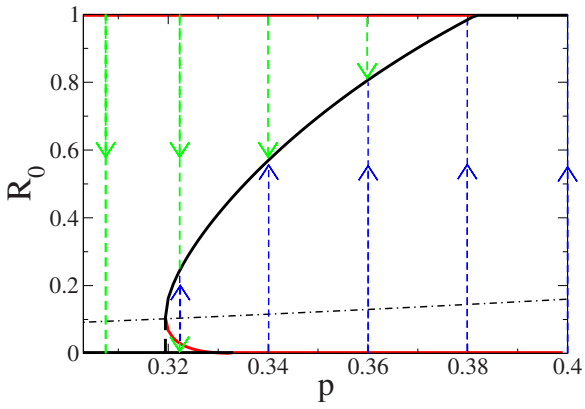

FIG. 15. (Color online) Phase diagram for the RG flow of HN-NP due to Eq. (37). Here, the all-connected operator *R* is used as in indicator of percolative order in the system. For any given *p*, R_n evolves along the shown trajectories starting from an initial value R_0. The homogeneous choice of bond probabilities in the network given in Eq. (21), i.e., $R_0=p^2$ along the (dash-dotted) diagonal line, crosses the line of unstable fixed points *just below* the branch-point singularity.

At first glance, the phase diagram for HN-NP appears to have "cured" all the unusual small-world effects of the previous networks and reverted to ordinary mean-field-like behavior: There is a domain for small $p \ge 0$ where the percolation probability vanishes and one at larger $p \le 1$ where percolation is certain, with what seems to be the usual 0–1 transition in the probability at some critical p_c (see, e.g., Fig. 17 in Ref. [1].). Yet, closer inspection of a relatively narrow regime near that transition, about for $0.3 < p < 0.4$, reveals a more subtle behavior. If we didn't have the exact RG equations in Eq. (37) available, a numerical simulation may well have missed it due to finite-size corrections. Within that narrow region, enlarged in Fig. 15, the resulting phase diagram is similar to Fig. 8, with a branch point where two lines of stable and unstable fixed points merge and disappear into the complex domain. But this branch point is oriented in the opposite direction, with a (minute) jump in the percolation probability at $\bar{p}_l=0.319\,445\,181\ldots$ preceding a continuous rise toward, again, $\bar{p}_u=2-\phi=0.381\,966\ldots$ above which percolation is certain. Unlike for Fig. 8, $R^*=0$ and $R^*=1$ are *always* fixed points (variably stable or unstable) for all *p*: while in the 2*d* hierarchical lattice the small-world bond for any *p* can bootstrap even the empty network into a spanning cluster with finite probability, in HN-NP this is only possible for a disconnected network when $p > \bar{p}_m = \frac{1}{3}$.

The analysis near the fixed points provides more details about these observations. The results for the fixed point at $R^*=1$ for $p < \bar{p}_u$ is identical to that for HN5 in Sec. IV B [see Eq. (33)] and provides again $\bar{p}_u=2-\phi$ as the transition point between the line of unstable and stable fixed points. In turn, the analysis near $R^*=0$, is different. Enforcing the norm constraint $N_n=1-R_n-S_n-U_n$ and expanding with the Ansatz

$$R_n \sim r_n^{(1)}, \quad (r_n^{(1)} \ll 1),$$

$$S_n \sim s_n^{(1)}, \quad (s_n^{(1)} \ll 1),$$

$$U_n \sim u_n^{(1)}, \quad (u_n^{(1)} \ll 1), \tag{38}$$

around the unstable fixed point to first order leads to

$$r_{n+1}^{(1)} \sim 2pr_n^{(1)},$$

$$s_{n+1}^{(1)} \sim 2(1-p)r_n^{(1)} + ps_n^{(1)} + 2u_n^{(1)},$$

$$u_{n+1}^{(1)} \sim ps_n^{(1)}. \tag{39}$$

The first relation immediately yields

$$r_n^{(1)} \sim (2p)^n r_0^{(1)}, \tag{40}$$

and the physically relevant solution for the remaining coupled set of linear recursions provides

$$s_n^{(1)} \sim u_n^{(1)} \sim A\left[\frac{p}{2}\left(1+\sqrt{1+\frac{8}{p}}\right)\right]^n. \tag{41}$$

(The modulus of the second, oscillatory, solution decays with n for all $0 \le p \le 1$.) Again, the highly nontrivial scaling exponent derived from Eq. (41) is nonuniversal. For small $p < \bar{p}_m = \frac{1}{3}$, all corrections decay and the fixed point remains stable. For $p > \bar{p}_m$, the solutions for $s_n^{(1)}$ and $u_n^{(1)}$ first become divergent, enough to make the fixed point itself unstable. Yet, $r_n^{(1)}$ initially remains convergent, slowing the RG flow. For $p > \frac{1}{2}$, the fixed point rapidly becomes unstable. The analysis of the branch point at $\bar{p}_l$ can only be done numerically because it involves the solution of sufficiently high-order polynomials to defy an explicit treatment.

V. CONCLUSIONS

We have obtained the exact phase diagrams for bond percolation on variants of the Hanoi networks using RG. For a small fraction of long-range bonds and a regular degree distribution, as in HN3, the network is finitely ramified and percolation requires a full bond density, $p_c = 1$. The hierarchical structure there manifests itself only in the finite-size corrections. Adding more long-range bonds at the price of obtaining an exponential degree distribution but a mean-field-like logarithmic distance between sites results in the network HN5. There, it leads to the unusual phenomenon of percolation with a finite probability, which we dubbed "patchy" order, facilitated by the addition of ever more long-range bonds at higher levels of the hierarchy that can reconnect patches of localized clusters at lower levels of the hierarchy. Introducing a nonplanar version of a Hanoi network provides nearly ideal mean-field behavior, with a completely disordered phase at low bond density and a fully ordered phase at high density. Yet, even here a narrow window with mixed behavior intervenes.

Here, we have all but scratched the surface of the analysis of percolation on small-world networks. In light of the ever increasing importance of small-world networks, practical and conceptual, we will focus on exploring further characteristics, such as details of clustering behaviors and correlations, on the variety of network configurations represented here. Only then can we hope to find solid classifications on the possible behaviors found in the real world. For instance, it might be possible to find recently observed discontinuous transitions in the size of spanning clusters ("explosive" percolation [31–34]) also in the neighborhood of the branch points of these merely hierarchically constructed networks. In particular, we are currently focused on a detailed study of the transitions in HN-NP [35] and a comparison with the classification considered in Ref. [27].

Possible extensions of this work to distance-dependent small-world bonds, and to other statistical models, are immediately apparent. In fact, it proves to be even simpler to solve the Ising model on Hanoi networks [28]. Similar patchy behavior is observed, where long-range bonds maintain a nonzero magnetization at the highest levels in the hierarchy at any finite temperature while ever larger domains of low-level spins have already decorrelated. In scale-free or nonequilibrium networks [25], this phenomenon has previously been interpreted as a Berezinskii-Kosterlitz-Thouless (BKT) transition that is "inverted" (as it appears in the disordered phase). On HN-NP we find a one-parameter solution which interpolates between a second-order transition and BTK.

ACKNOWLEDGMENTS

S.B. acknowledges support from the U.S. National Science Foundation through Grant No. DMR-0812204 and R.M.Z. through Grant No. DMS-0553487.

APPENDIX: SECOND-ORDER CORRECTION TO $p_c = 1$ IN HN3

We expand around the unstable fixed point (0,1,0,0) of the RG recursions [Eq. (19)] for HN3 to second order with the Ansatz,

$$R_n \sim 1 - r_n^{(1)} + r_n^{(2)}, \quad (r_n^{(2)} \ll r_n^{(1)} \ll 1),$$

$$S_n \sim r_n^{(1)} + s_n^{(2)}, \quad (s_n^{(2)} \ll r_n^{(1)} \ll 1),$$

$$U_n \sim u_n^{(2)}, \quad (u_n^{(2)} \ll r_n^{(1)} \ll 1),$$

$$N_n \sim \eta_n^{(2)}, \quad (\eta_n^{(2)} \ll r_n^{(1)} \ll 1), \tag{42}$$

where we have used Eq. (25) to eliminate $s_n^{(1)}$ in favor of $r_n^{(1)}$. Of course, all terms of lower order cancel, and after dropping terms of higher than second order, we arrive at

$$r_{n+1}^{(2)} \sim 2r_n^{(2)} + 2u_n^{(2)} + ps_n^{(2)} + (1-p)(r_n^{(1)})^2,$$

$$s_{n+1}^{(2)} \sim (2-p)s_n^{(2)} + 2\eta_n^{(2)} + \left(\frac{3}{2}p - 2\right)(r_n^{(1)})^2,$$

$$u_{n+1}^{(2)} \sim \frac{p}{4}(r_n^{(1)})^2,$$

$$\eta_{n+1}^{(2)} \sim \left(1 - \frac{3}{4}p\right)(r_n^{(1)})^2, \tag{43}$$

assuming that squares of terms of first order are of second order. The solutions for $u_n^{(2)}$ and $\eta_n^{(2)}$ are

$$u_n^{(2)} = \frac{p}{4}A^2(2-p)^{2n-2},$$

$$\eta_n^{(2)} = \left(1 - \frac{3}{4}p\right)A^2(2-p)^{2n-2}. \tag{44}$$

Inserting these results into the equation for $s_{n+1}^{(2)}$ yields

$$s_{n+1}^{(2)} \sim (2-p)s_n^{(2)} + \left(2 - \frac{3}{2}p\right)[1-(2-p)^2]A^2(2-p)^{2n-2}. \tag{45}$$

The inhomogeneous term in this relation can be neglected at this order, in fact, as the expression in the square brackets vanishes in the limit $p \to 1$, and we are left with the same solution for $s_n^{(2)}$ as in first order,

$$s_n^{(2)} = B(2-p)^n, \tag{46}$$

where $B \ll A$. (In fact, we expect $B/A \sim \epsilon_k$.)

Regarding the relation for $r_n^{(2)}$ in Eq. (43), we can drop the last term in this order as $1-p \to 0$ and find

$$r_{n+1}^{(2)} \sim 2r_n^{(2)} + 2u_n^{(2)} + ps_n^{(2)},$$

$$\sim 2r_n^{(2)} + \frac{p}{2}A^2(2-p)^{2n-2} + pB(2-p)^n. \tag{47}$$

The homogeneous solution of this relation at $n=-k$ would decay exponentially, $\sim 2^{-k}$, and can be discarded, leaving us with

$$r_n^{(2)} \sim \frac{p}{2}A^2(2-p)^{2n-4} + pB(2-p)^{n+1}. \tag{48}$$

Inserting the second-order solutions in Eqs. (44), (46), and (48) together with the results from Sec. IV A into Eq. (42) and evaluating at $n=k$, we get

$$R_{-k} \sim 1 - A(2-p)^{-k} + pB(2-p)^{-k-1} + \frac{p}{2}A^2(2-p)^{-2k-4},$$

$$S_{-k} \sim A(2-p)^{-k} + B(2-p)^{-k}, \quad (A \gg B),$$

$$U_{-k-1} \sim \frac{p}{4}A^2(2-p)^{-2k},$$

$$N_{-k} \sim \left(1 - \frac{3}{4}p\right)A^2(2-p)^{-2k-2}. \tag{49}$$

We extend the correction on p_c to second order, i.e.,

$$p \sim 1 - \epsilon_k + b\epsilon_k^2, \tag{50}$$

where $b=b(\epsilon_k)$ should only vary weakly with ϵ_k. Inserted into Eq. (49), we get

$$R_{-k} \sim 1 - 2\epsilon_k + \epsilon_k^2\left[2 + 2b\ln\left(\frac{2\epsilon_k}{A}\right) + 2\frac{B}{\epsilon_k A}\right],$$

$$S_{-k} \sim 2\epsilon_k + \epsilon_k^2\left[-2b\ln\left(\frac{2\epsilon_k}{A}\right) + 2\frac{B}{\epsilon_k A}\right],$$

$$U_{-k+1} \sim \epsilon_k^2,$$

$$N_{-k} \sim \epsilon_k^2, \tag{51}$$

where we used

$$A(2-p)^{-k} \sim A(1+\epsilon_k - b\epsilon_k^2)^{-k},$$

$$\sim A(1+\epsilon_k)^{-k}(1+bk\epsilon_k^2),$$

$$\sim 2\epsilon_k\left[1 - b\ln\left(\frac{2\epsilon_k}{A}\right)\epsilon_k\right], \tag{52}$$

because Eq. (29) yields $-k\epsilon_k \sim \ln(2\epsilon_k/A)$.

Correspondingly, we can expand the initial conditions

$$R_{-k} = p^2 \sim 1 - 2\epsilon_k + \epsilon_k^2(1+2b),$$

$$S_{-k} = 2p(1-p) \sim 2\epsilon_k + \epsilon_k^2(-2-2b),$$

$$N_{-k} = (1-p)^2 \sim \epsilon_k^2. \tag{53}$$

Note that in Eq. (51) we have used the result for the newly emerging operator U at $n=k-1$, because U_{-k} itself would strictly vanish to all orders. But with the help of its relation in Eq. (19), we obtain via the initial condition for S_n,

$$U_{-k+1} = p^3(1-p)^2 \sim \epsilon_k^2. \tag{54}$$

Comparison of those results with Eq. (51) proves the consistency for N and U. As expected from Sec. IV A, the relations for R and S are also consistent immediately up to first order. Requiring consistency to second order provides the relations

$$1 + 2b = 2 + 2b\ln\left(\frac{2\epsilon_k}{A}\right) + 2\frac{B}{\epsilon_k A},$$

$$-2 - 2b = -2b\ln\left(\frac{2\epsilon_k}{A}\right) + 2\frac{B}{\epsilon_k A},$$

that determine the integration constant B and, more importantly, the second-order correction b to p_c,

$$b = -\frac{1}{4}\frac{1}{1+\ln\left(\frac{A}{2\epsilon_k}\right)}, \quad B = -\frac{3}{4}\epsilon_k A. \tag{55}$$

A redundant test of these results is provided by the normalization constraint,

$$1 = R_{-k} + S_{-k} + N_{-k}, \tag{56}$$

which we find satisfied to second order. (Remember that $U_{-k}=0$.)

Hence, we obtain finally for the finite-size corrections of p_c,

$$p_c \sim 1 - \epsilon_k - \frac{1}{4}\frac{1}{1+\ln\left(\frac{A}{2\epsilon_k}\right)}\epsilon_k^2 + \cdots, \tag{57}$$

where the relation in Eq. (29), $A(1+\epsilon_k)^{-k} \sim 2\epsilon_k$, defines ϵ_k. Unfortunately, we do not see any way to determine the arbitrary constant A in this expansion. We assume that it is a reflection of the local nature of our expansion for $k \to \infty$ [36]. It seems that A would have to be determined from global information about the solution, such as from an evaluation at $n=0$.

[1] D. Stauffer and A. Aharony, *Introduction to Percolation Theory*, 2nd ed. (C. R. C. Press, Boca Raton, FL, 1994).
[2] M. Sahimi, *Applications of Percolation Theory* (Taylor & Francis, New York, 1994).
[3] M. B. Isichenko, Rev. Mod. Phys. **64**, 961 (1992).
[4] P. G. de Gennes J. Phys. Lett. **37**, 1 (1976).
[5] S. Boccaletti, V. Latora, Y. Moreno, M. Chavez, and D.-U. Hwang, Phys. Rep. **424**, 175 (2006).
[6] P. Erdős and A. Rényi, *The Art of Counting* (MIT, Cambridge, 1973).
[7] B. Bollobas, *Random Graphs* (Academic Press, London, 1985).
[8] A.-L. Barabasi, *Linked* (Plume Books, New York, 2003).
[9] M. E. J. Newman, SIAM Rev. **45**, 167 (2003).
[10] S. Boettcher, B. Gonçalves, and H. Guclu, J. Phys. A: Math. Theor. **41**, 252001 (2008).
[11] S. Boettcher and B. Goncalves, EPL **84**, 30002 (2008).
[12] S. Boettcher, B. Goncalves, and J. Azaret, J. Phys. A: Math. Theor. **41**, 335003 (2008).
[13] M. Plischke and B. Bergersen, *Equilibrium Statistical Physics*, 2nd ed. (World Scientific, Singapore, 1994).
[14] A.-L. Barabási and R. Albert, Science **286**, 509 (1999).
[15] J. S. Andrade, H.-J. Herrmann, R. F. S. Andrade, and L. R. da Silva, Phys. Rev. Lett. **94**, 018702 (2005).
[16] Z. Zhang, S. Zhou, L. Fang, J. Guan, and Y. Zhang, EPL **79**, 38007 (2007).
[17] D. J. Watts and S. H. Strogatz, Nature (London) **393**, 440 (1998).
[18] M. E. J. Newman and D. J. Watts, Phys. Lett. A **263**, 341 (1999).
[19] L. Leuzzi, G. Parisi, F. Ricci-Tersenghi, and J. J. Ruiz-Lorenzo, Phys. Rev. Lett. **101**, 107203 (2008).
[20] A. A. Migdal, J. Exp. Theor. Phys. **42**, 743 (1976).
[21] L. P. Kadanoff, Ann. Phys. **100**, 359 (1976).
[22] A. N. Berker and S. Ostlund, J. Phys. C **12**, 4961 (1979).
[23] M. Hinczewski and A. N. Berker, Phys. Rev. E **73**, 066126 (2006).
[24] A. Nihat Berker, M. Hinczewski, and R. R. Netz, Phys. Rev. E (to be published).
[25] S. N. Dorogovtsev, A. V. Goltsev, and J. F. F. Mendes, Rev. Mod. Phys. **80**, 1275 (2008).
[26] M. Kaufman and R. B. Griffiths, Phys. Rev. B **28**, 3864 (1983).
[27] T. Nogawa and T. Hasegawa, J. Phys. A: Math. Theor. **42**, 145001 (2009).
[28] S. Boettcher and T. Brunson (to be published).
[29] M. Livio, *The Golden Ratio* (Broadway Books, New York, 2003).
[30] H. Taitelbaum, S. Havlin, P. Grassberger, and U. Moening, J. Phys. A **23**, 371 (1990).
[31] D. Achlioptas, R. M. D'Souza, and J. Spencer, Science **323**, 1453 (2009).
[32] R. M. Ziff, Phys. Rev. Lett. **103**, 045701 (2009).
[33] Y. Cho, J. Kim, J. Park, B. Kahng, and D. Kim, Phys. Rev. Lett. **103**, 135702 (2009).
[34] F. Radicchi and S. Fortunato, Phys. Rev. Lett. (to be published).
[35] R. M. Ziff and S. Boettcher (to be published).
[36] C. M. Bender and S. A. Orszag, *Advanced Mathematical Methods for Scientists and Engineers* (McGraw-Hill, New York, 1978).